



**RESEARCH ARTICLE**

# Temporospatial distribution and transcriptional profile of retinal microglia in the oxygen-induced retinopathy mouse model

Myriam Boeck<sup>1</sup> | Adrian Thien<sup>1</sup> | Julian Wolf<sup>1</sup> | Nora Hagemeyer<sup>2</sup> |  
 Yannik Laich<sup>1</sup> | Dilmurat Yusuf<sup>3</sup> | Rolf Backofen<sup>3</sup> | Peipei Zhang<sup>1</sup> |  
 Stefaniya Boneva<sup>1</sup> | Andreas Stahl<sup>4</sup> | Ingo Hilgendorf<sup>5</sup> | Hansjürgen Agostini<sup>1</sup> |  
 Marco Prinz<sup>2,6,7</sup>  | Peter Wieghofer<sup>8</sup> | Günther Schlunck<sup>1</sup> | Anja Schlecht<sup>1</sup> |  
 Clemens Lange<sup>1</sup> 

<sup>1</sup>Eye Center, Medical Center, Faculty of Medicine, University of Freiburg, Freiburg im Breisgau, Germany

<sup>2</sup>Institute of Neuropathology, Faculty of Medicine, University of Freiburg, Freiburg im Breisgau, Germany

<sup>3</sup>Department of Bioinformatics, University of Freiburg, Freiburg im Breisgau, Germany

<sup>4</sup>Department of Ophthalmology, University Medical Center Greifswald, Greifswald, Germany

<sup>5</sup>Cardiology and Angiology, University Heart Center, University of Freiburg, Freiburg im Breisgau, Germany

<sup>6</sup>Signalling Research Centres BIOS and CIBSS, University of Freiburg, Freiburg im Breisgau, Germany

<sup>7</sup>Center for Basics in NeuroModulation (NeuroModulBasics), Faculty of Medicine, University of Freiburg, Freiburg im Breisgau, Germany

<sup>8</sup>Institute of Anatomy, University of Leipzig, Freiburg im Breisgau, Germany

**Correspondence**

Anja Schlecht and Clemens Lange, Eye Center, Medical Center, Faculty of Medicine, University of Freiburg, Freiburg im Breisgau, Germany.

Email: anja.schlecht@uniklinik-freiburg.de (A. S.) and clemens.lange@uniklinik-freiburg.de (C. L.)

**Funding information**

Deutsche Forschungsgemeinschaft, Grant/Award Number: SFB/TRR167; Else-Kröner-Fresenius Foundation

**Abstract**

Myeloid cells such as resident retinal microglia (MG) or infiltrating blood-derived macrophages (M $\phi$ ) accumulate in areas of retinal ischemia and neovascularization (RNV) and modulate neovascular eye disease. Their temporospatial distribution and biological function in this process, however, remain unclarified. Using state-of-the-art methods, including cell-specific reporter mice and high-throughput RNA sequencing (RNA Seq), this study determined the extent of MG proliferation and M $\phi$  infiltration in areas with retinal ischemia and RNV in *Cx3cr1<sup>CreERT2</sup>;Rosa26-tdTomato* mice and examined the transcriptional profile of MG in the mouse model of oxygen-induced retinopathy (OIR). For RNA Seq, tdTomato-positive retinal MG were sorted by flow cytometry followed by Gene ontology (GO) cluster analysis. Furthermore, intraperitoneal injections of the cell proliferation marker 5-ethynyl-2'-deoxyuridine (EdU) were performed from postnatal day (p) 12 to p16. We found that MG is the predominant myeloid cell population while M $\phi$  rarely appears in areas of RNV. Thirty percent of retinal MG in areas of RNV were EdU-positive indicating a considerable local MG cell

Anja Schlecht and Clemens should be considered joint senior authors

This is an open access article under the terms of the Creative Commons Attribution-NonCommercial-NoDerivs License, which permits use and distribution in any medium, provided the original work is properly cited, the use is non-commercial and no modifications or adaptations are made.

© 2020 The Authors. *Glia* published by Wiley Periodicals, Inc.



expansion. GO cluster analysis revealed an enrichment of clusters related to cell division, tubulin binding, ATPase activity, protein kinase regulatory activity, and chemokine receptor binding in MG in the OIR model compared to untreated controls. In conclusion, activated retinal MG alter their transcriptional profile, exhibit considerable proliferative ability and are by far the most frequent myeloid cell population in areas of ischemia and RNV in the OIR model thus presenting a potential target for future therapeutic approaches.

#### KEYWORDS

*Cx3cr1<sup>CreERT2</sup>*, microglia, oxygen-induced retinopathy, retinal neovascularization, RNA sequencing

## 1 | INTRODUCTION

Retinal neovascularization (RNV) is a common feature in patients with retinopathy of prematurity, retinal vein occlusion, and proliferative diabetic retinopathy, which are among the leading causes of blindness worldwide (Sapieha et al., 2010). RNV can cause retinal and vitreous bleeding, edema formation, and tractional retinal detachments which in turn can lead to irreversible blindness if left untreated. The cellular and molecular mechanisms underlying RNV formation are not fully understood and an optimal treatment has not yet been established. The introduction of therapies targeting the vascular endothelial growth factor (VEGF) has enabled significant progress in the treatment of patients with RNV, especially in retinopathy of prematurity (Figueira et al., 2018; Stahl et al., 2018). However, about 56% of diabetic patients with proliferative diabetic retinopathy demonstrate persistent RNV despite intensive anti-VEGF therapy and panretinal photocoagulation (Figueira et al., 2018), highlighting the disease's complexity and pointing towards other unaddressed disease-associated cellular and molecular mechanisms.

Recent advances in our understanding of the pathogenesis of ischemia-induced RNV have identified myeloid cells as key modulators of disease progression. Myeloid cells, such as resident microglia (MG) and recruited monocyte-derived macrophages (M $\phi$ ) from the blood, accumulate in areas of ischemia and RNV and have been suggested to be a driving force for disease progression (Green, 1991; Zeng, Green, & Tso, 2008). The degree to which different subtypes of myeloid cells contribute to RNV formation or regression, however, is undetermined. This is to a large extent due to the fact that resident MG and blood-derived M $\phi$  cannot be differentiated based on the expression of cell surface markers (Sousa, Biber, & Michelucci, 2017).

In this study, we used MG cell-specific reporter mice to dissect the temporospatial distribution of resident MG and infiltrating M $\phi$  and to assess the proliferative capacity of MG in a mouse model of ischemia-induced RNV. Furthermore, we exploited high-throughput RNA Seq of isolated MG to investigate their expression profile in the steady state as well as during retinal ischemia and RNV formation. In contrast to the prevailing notion, we found that resident MG

proliferate and constitute the predominant myeloid cell population in areas of ischemia and RNV, while the number of blood-derived M $\phi$  is substantially lower.

## 2 | MATERIALS AND METHODS

### 2.1 | Mice

All animal experiments were approved by our local authority (Regierungspräsidium Freiburg, Germany) and conformed to EU Directive 2010/63/EU. *Cx3cr1<sup>CreERT2</sup>* and *Rosa26-fl-stop-fl-tdTomato* (*Rosa26-tdTomato*) mice were bred on a C57BL/6J background under specific pathogen-free conditions. *Cx3cr1<sup>CreERT2</sup>* mice were crossed to *Rosa26-tdTomato* mice to generate experimental *Cx3cr1<sup>CreERT2</sup>; Rosa26-tdTomato* mice. C57BL/6J mice were used for protein and cytokine analysis. All mice used in this study were negative for the *Rd8* (*Crb1*) mutation.

### 2.2 | Tamoxifen treatment

To induce nuclear CreER recombinase activity, young *Cx3cr1<sup>CreERT2</sup>; Rosa26-tdTomato* mice were given a subcutaneous injection of 5  $\mu$ l of 21 mg/ml tamoxifen (TAM, T5648-1G, Sigma-Aldrich, Taufkirchen, Germany) dissolved in corn oil (C8267, Sigma-Aldrich) at postnatal day p1. Corn oil- and phosphate-buffered saline (PBS)-injected mice served as controls.

### 2.3 | Oxygen-induced retinopathy mouse model

Mouse pups and their nursing dam were kept in an oxygen supply chamber at  $75 \pm 3\%$  O<sub>2</sub> from p7 to p12 and subsequently returned to room air as previously described (C. Lange et al., 2009). All mice were raised and kept at a constant temperature with a 12 hr light/dark cycle. The bodyweight of each pup was closely monitored to ascertain adequate metabolic health (Stahl et al., 2010). Pups were perfused

with PBS as described below and culled by cervical translocation at p7, p10, p12, or p17. Control mice (nOIR) were kept in room air and sacrificed at respective time points.

## 2.4 | Fluorescence microscopy

After intracardiac perfusion with PBS followed by 4% paraformaldehyde (PFA), eyes were fixed in 4% PFA for 1 hr at 4°C and processed for flat-mounts as described previously (Wang et al., 2013). Primary antibodies against IBA1 (AB178846, Abcam, Cambridge, United Kingdom; 019-19741, WAKO, Osaka, Japan; 234004, Synaptic Systems, Göttingen, Germany), TMEM119 (400002, Synaptic Systems) or Collagen IV (COL4, AB769, Merck Millipore, Billerica, MA) were added over two nights at a dilution of 1:500 at 4°C. Secondary antibodies were added at a dilution of 1:500 (Alexa Fluor® 647 and Alexa Fluor® 488, Life Technologies, Carlsbad, CA) overnight at 4°C. Images of the entire retina were taken using a Hamamatsu NanoZoomer S60 (Hamamatsu Photonics, Herrsching, Germany) to assess the retinal vasculature. To quantify MG cell numbers, confocal images were taken using a Leica SP8 confocal microscope (Leica, Wetzlar, Germany).

## 2.5 | Identification of microglia and blood-derived macrophages

Confocal images of the peripheral retina (P), the vaso-obliterative zone (VO) and area of RNV were imaged as described above and compared to retinal mid-periphery of control nOIR animals. IBA1<sup>+</sup> cells were quantified in the ganglion cell layer plus the inner plexiform layer (GCL + IPL) as well as in the outer plexiform layer (OPL) using Fiji ImageJ (Schindelin et al., 2012). Resident MG cells were defined as IBA1<sup>+</sup>tdTomato (Tom)<sup>+</sup> cells and blood-derived infiltrating Mφ as IBA1<sup>+</sup>Tom<sup>-</sup>. The percentage of Tom<sup>+</sup> cells was determined among all IBA1<sup>+</sup> cells.

## 2.6 | In vivo EdU proliferation assay

EdU (50 µg per day at a concentration of 125 µg EdU per 100 µl PBS) was applied intraperitoneally on five consecutive days from p12 to p16 in oxygen-induced retinopathy (OIR)-treated *Cx3cr1<sup>CreERT2</sup>; Rosa26-tdTomato* mice. Mice were sacrificed at p17. Intracardiac perfusion, eye fixation, and flat-mount preparation were performed as described above. EdU was visualized by the Click-iT™ EdU Alexa Fluor™ 647 Imaging Kit (C10340, Thermo Fisher Scientific, Waltham, MA) according to the manufacturer's protocol followed by anti-Collagen IV staining as described above.

## 2.7 | Flow cytometry

Eyecups of PBS-perfused mice were dissected to separate the retina from adjacent tissue. Retinal tissue was dissociated by resuspension.

Peripheral blood samples were obtained by heart puncture. Dead cells were excluded by incubation in fixable viability dye 506 (65-0866-14, eBioscience, Thermo Fisher Scientific). Anti-CD16/CD32 Fc block (553142, BD Pharmingen, BD Biosciences, Franklin Lakes, NJ) was performed at 4°C for 20 min at a concentration of 1:200 to avoid unspecific binding. Cells were stained with antibodies directed against CD45 (30-F11, 103133, BioLegend, San Diego, CA), CD11b (M1/70, 17-0112-83, eBioscience, Thermo Fisher Scientific), Ly6C (AL-21, 45-5932-82, eBioscience, Thermo Fisher) and Ly6G (1A8, 551460, BD Pharmingen, BD Biosciences) at 4°C for 20 min at a concentration of 1:200. For blood analysis, 50 µl of blood were lysed using RBC Lysis Buffer (00-4333-57, eBioscience, Thermo Fisher Scientific). Anti-CD16/CD32 Fc block was performed at 4°C for 20 min at a concentration of 1:200 to avoid unspecific binding. Cells were stained with primary antibodies directed against CD45 (30-F11), CD11b (M1/70), CD115 (1:100, 25-1152-82, eBioscience, Thermo Fisher Scientific), Ly6C (AL-21) and Ly6G (1A8) at 4°C for 20 min at a concentration of 1:200 in the dark. Cells were washed and analyzed using a FACSCanto II (BD Biosciences) for blood samples and MoFlo Astrios EQ (Beckman Coulter, Brea, CA) to sort retinal cells. To obtain an average of 10,000 retinal MG per sample for RNA Seq analysis the retinas of 2 to 3 mice were FACS-sorted and pooled. The retina of one mouse per OIR litter was used to confirm an efficient induction of RNV and VO via immunofluorescence before performing RNA Seq experiments. Data were acquired with FACSDiva software (BD Pharmingen, BD Biosciences). Post-acquisition analysis was performed using FlowJo software (Tree Star, Inc., Ashland, OR).

## 2.8 | Total RNA extraction

RNA extraction, library preparation, and RNA Seq were performed at the Genomics Core Facility "KFB - Center of Excellence for Fluorescent Bioanalytics" (University of Regensburg, Germany; www.kfb-regensburg.de). In brief, eyes were enucleated and total RNA was extracted from isolated retinal MG and stabilized in RNA protect buffer according to the RNeasy Plus Micro Kit protocol (74004, QIAGEN, Hilden, Germany). Retinal MG were stored and shipped in RNA protect buffer at 2–8°C. After pelleting, the RNA protect buffer was removed and replaced by RLT Plus and the samples were homogenized by vortexing for 30 s. Genomic DNA contamination was eliminated using gDNA Eliminator spin columns. Next, ethanol was added, and the samples were applied to RNeasy MinElute spin columns followed by several wash steps. Finally, total RNA was eluted in 12 µl of nuclease-free water. The RNA's purity and integrity were determined on the Agilent 2100 Bioanalyzer with the RNA 6000 Pico LabChip reagent set (5067-1513, Agilent, Palo Alto, CA).

## 2.9 | RNA sequencing

In total 8 OIR and 8 nOIR microglia samples were analyzed using RNA Seq. The SMARTer Ultra Low Input RNA Kit for Sequencing v4

(Clontech Laboratories, Inc., Mountain View, CA) was used to generate first-strand cDNA from 750 pg total RNA. Double-stranded cDNA was amplified by LD PCR (12 cycles) and purified via magnetic bead clean-up. Library preparation was carried out as described in the Illumina Nextera XT Sample Preparation Guide (Illumina, Inc., San Diego, CA). Then, 150 pg of input cDNA were tagged (tagged and fragmented) by the Nextera XT transposome. The products were purified and amplified via a limited-cycle PCR program to generate multiplexed sequencing libraries. For the PCR step 1:5 dilutions of index 1 (i7) and index 2 (i5) primers were used. The libraries were quantified using the KAPA SYBR FAST ABI Prism Library Quantification Kit (Kapa Biosystems, Inc., Woburn, MA). Equimolar amounts of each library were pooled and the pools then used for cluster generation on the cBot with the TruSeq SR Cluster Kit v3 (GD-401-3001, Illumina, Cambridge, UK). The sequencing run was performed on a HiSeq 1000 instrument using the indexed 50 cycles single-read (SR) protocol and TruSeq SBS v3 Reagents according to the Illumina HiSeq 1000 System User Guide. Image analysis and base calling resulted in bcl files which were converted into fastq files with the bcl2fastq v2.18 software. These sequence data have been submitted to the Gene Expression Omnibus database under accession number GSE132731. Address is as follows: <https://www.ncbi.nlm.nih.gov/geo/query/acc.cgi?acc=GSE132731>. The password is available from the corresponding author upon request.

## 2.10 | Differential gene expression analysis and data visualization

Sequencing data were uploaded to the public Galaxy web platform (<https://usegalaxy.org>) to analyze the data (Afgan et al., 2016). Quality control was performed with *FastQC Galaxy Version 0.72* (Andrews, 2018). Reads were mapped to the mouse genome (Gencode M20) with *RNA STAR Galaxy Version 2.6.0b-1* (Dobin et al., 2013) and counted using *featureCounts Galaxy Version 1.6.2* (Liao, Smyth, & Shi, 2014). Differential gene expression was analyzed using *DESeq2 Galaxy Version 2.11.40.2* (Love, Huber, & Anders, 2014). The output of DESeq2 was imported to GNU R 3.5.1 and checked for plausibility of results. Strict thresholds ( $\log_2$  fold change [ $\log_2FC$ ]  $\geq 1$  or  $\leq -1$ ,  $p < .01$ ) were applied to minimize false positives when interpreting the differentially expressed genes (DEG) between OIR and nOIR control MG. Data visualization with volcano plots was performed using the *ggplot2* package. Heatmaps were created with the R package *ComplexHeatmap 1.20.0* (Gu, Eils, & Schlesner, 2016). Gene enrichment analysis was done using the R package *clusterProfiler 3.10.1* (Yu, Wang, Han, & He, 2012).

## 2.11 | Protein analysis

Proteins were isolated from retinal tissue of OIR and nOIR control mice ( $n = 6$  per group) using RIPA buffer (R0278, Sigma-Aldrich) containing protease (Complete Tablets Mini, 0463159001, Roche, Basel, Switzerland) and phosphatase inhibitors (Phosstop, 04906845001,

Roche). The amount of recovered protein was evaluated via colorimetric assay (Pierce™ BCA Protein Assay Kit, 23225, Thermo Fisher Scientific). To examine cytokine concentrations in retinal samples, we used a multiarray electrochemiluminescence panel (R-Plex, Meso-Scale Discovery, Rockville, MD) according to the manufacturer's instructions. This kit simultaneously measured protein levels of Interleukin (IL) 1 beta (IL1b), IL6, IL16, CC-chemokine ligand (CCL) 2, CCL3, CCL4, tumor necrosis factor-alpha (TNFA), Transforming growth factor-beta 1 (TGFB1) and Vascular Endothelial Growth Factor A (VEGFA). These factors were chosen by relying on the RNA Seq results of this study and represented relevant DEG in OIR MG compared to steady-state MG. For statistical analysis, all values below the detection limit were assigned to the respective values of the detection limit.

## 2.12 | Statistical analysis

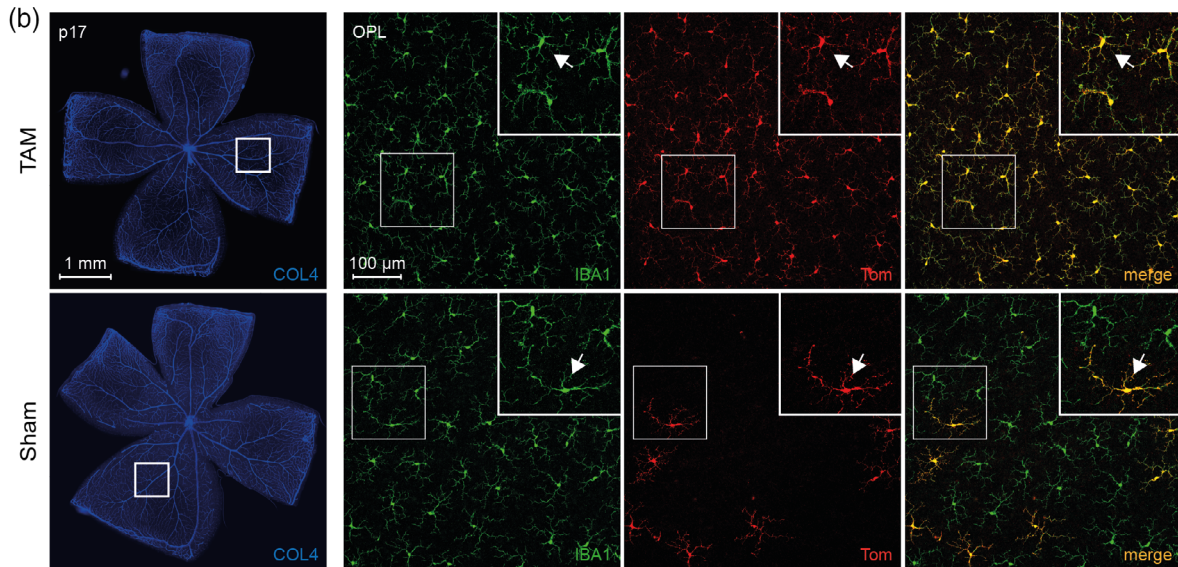
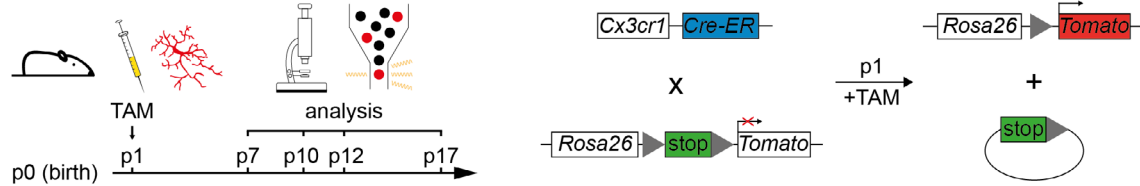
Statistical analysis was performed using GraphPad Prism (GraphPad Software, Version 6.0, La Jolla, CA). Data were tested for normality applying the D'Agostino-Pearson Omnibus test. If normality was given, an unpaired *t* test was applied. If the data did not meet the criteria of normality, the Mann-Whitney test was applied. Differences were considered significant when  $p$ -value  $< .05$ .

## 3 | RESULTS

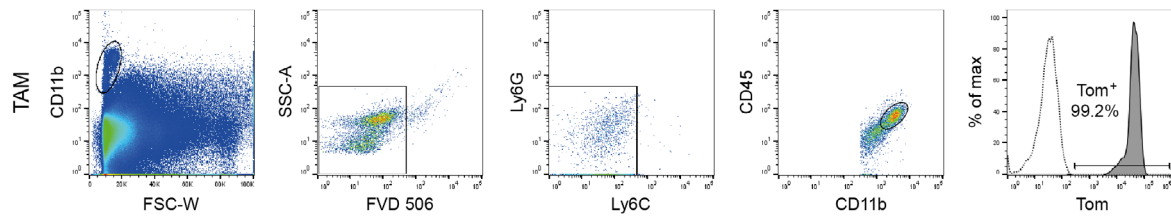
### 3.1 | Characterization of the *Cx3cr1<sup>CreERT2</sup>; Rosa26-tdTomato* line in the retina of young mice

In the past, discrimination between resident retinal microglia (MG) and peripheral blood-derived macrophages (M $\phi$ ) in the diseased retina was hampered by the lack of cell-specific markers and suitable mouse models. We recently demonstrated that *Cx3cr1<sup>CreERT2</sup>; Rosa26-YFP* mice allow to distinguish MG from infiltrating blood-derived M $\phi$  in the brain of adult mice (Goldmann et al., 2013). To validate the potential of this mouse model in young mice, we injected a single pulse of tamoxifen or diluent (sham) at p1 in new-born *Cx3cr1<sup>CreERT2</sup>; Rosa26-tdTomato* mice and assessed the recombination efficiency in retinal MG and in peripheral blood cells at p7, p10, p12, and p17 in the steady-state (Figure 1a). The immunofluorescence analysis of young *Cx3cr1<sup>CreERT2</sup>; Rosa26-tdTomato* mice revealed a regular pattern of ramified IBA1<sup>+</sup> MG cells demonstrating a high recombination efficiency of tdTomato at p7 (mean  $\pm$  SD =  $98.3 \pm 1.9\%$ ), p10 ( $99.4 \pm 0.4\%$ ), p12 ( $99.5 \pm 0.1\%$ ), and p17 ( $99.5 \pm 0.5\%$ ). Sham-injected *Cx3cr1<sup>CreERT2</sup>; Rosa26-tdTomato* mice in contrast, showed a low recombination efficiency at p7 ( $14.9 \pm 5.4\%$ ), p12 ( $21.0 \pm 5.5\%$ ), and p17 ( $24.3 \pm 5.4\%$ , Figure 1b,e), indicating tamoxifen-independent recombination events in the *Rosa26* locus which increase with age. In line with these results, flow-cytometry analysis of CD45<sup>lo</sup>CD11b<sup>+</sup>Ly6C<sup>-</sup>Ly6G<sup>-</sup> retinal MG at p17 confirmed high recombination efficiency of  $99.0\% (\pm 0.3\%)$  in the tamoxifen-treated group compared with  $23.9\% (\pm 2.0\%)$  in the

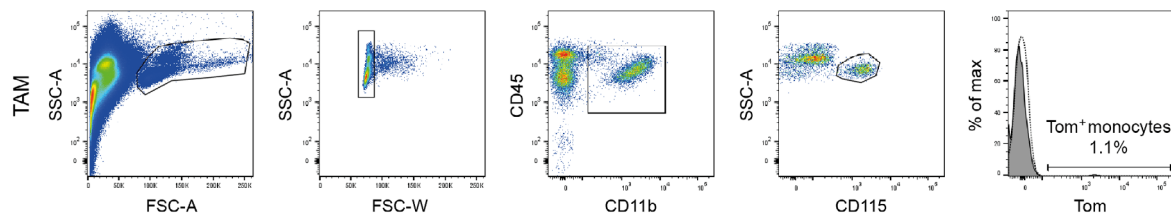


(a) *Cx3cr1<sup>CreERT2</sup>; Rosa26-tdTomato*

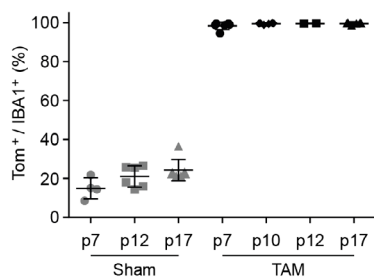
## (c) Retina p17: FACS



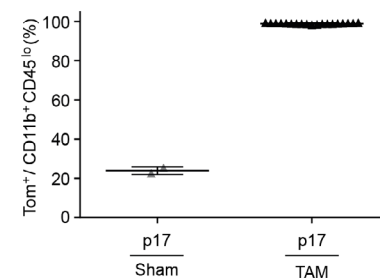
## (d) Blood p17: FACS



## (e) Retina: immunofluorescence



## (f) Retina: FACS



## (g) Blood: FACS

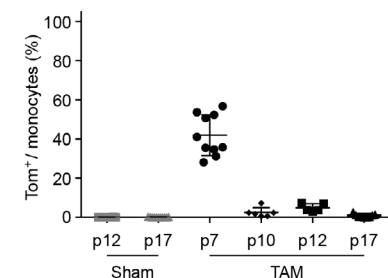


**FIGURE 1** Legend on next page.

sham-treated group (Figure 1c,f). Since tamoxifen injection of *Cx3cr1<sup>CreERT2</sup>;Rosa26-tdTomato* mice induces tdTomato expression in all *Cx3cr1*-expressing cells including peripheral monocytes, we next assessed the CreER recombination efficiency in peripheral blood monocytes at p7, p10, p12, and p17. Flow cytometry analysis of CD45<sup>hi</sup>CD11b<sup>+</sup>CD115<sup>+</sup>SSc<sup>lo</sup> peripheral blood monocytes revealed a decreasing percentage of tdTomato<sup>+</sup> peripheral monocytes over time following tamoxifen treatment. While 42.0% ( $\pm$  10.4%) of the monocytes expressed tdTomato at p7, this number decreased to 2.5% ( $\pm$  2.5%) at p10, 4.9% ( $\pm$  2.5%) at p12, and 0.8% ( $\pm$  0.9%) at p17 indicating a rapid cell turnover of peripheral monocytes that are constantly renewed by *Cx3cr1*-negative precursor cells in the bone marrow (Figure 1d,g).

Taken together, these data demonstrate that early (p1) single-pulse tamoxifen treatment of *Cx3cr1<sup>CreERT2</sup>;Rosa26-tdTomato* mice induces efficient and persistent tdTomato expression in virtually all resident retinal MG while the labeling of circulating monocytes rapidly subsides over time due to steady turnover of these cells. This strategy allows discriminating retinal MG and infiltrating M $\phi$  in young mice in the OIR model.

### 3.2 | Temporospatial distribution of myeloid subsets during retinal ischemia and neovascularization in the OIR mouse model

To study the temporospatial distribution of resident retinal MG and infiltrating M $\phi$  in the ischemic retina and in areas of RNV, we injected tamoxifen in *Cx3cr1<sup>CreERT2</sup>;Rosa26-tdTomato* mice at p1 and assessed the number of retinal MG and blood-derived infiltrating M $\phi$  at p10, p12, and p17 in the OIR model (Figure 2a).

Immunofluorescence microscopy revealed that the morphology and distribution pattern of myeloid cells changed considerably in the OIR model. IBA1<sup>+</sup> retinal myeloid cells displayed an amoeboid and less-ramified morphology indicating an activated state (Figure 2b). At p10 similar numbers of IBA1<sup>+</sup> retinal myeloid cells were observed in the periphery and vaso-obliterative area in the OIR group compared

with the nOIR group (Figure 2c). At p12, however, the absolute number of IBA1<sup>+</sup> retinal myeloid cells was substantially increased in the periphery and vaso-obliterative area in the OIR group compared to the nOIR group (Figure 2c) indicating an onset of MG cell expansion or migration between p10 and p12. Interestingly, only neglectable numbers of IBA1<sup>+</sup>Tom<sup>-</sup> cells were detectable in the peripheral retina and VO at p10 and p12 (Figure 2c, Figure S1) suggesting a low infiltration of blood-derived monocytes during this time. The distribution of myeloid cells changed dramatically with the onset of RNV, which in the OIR model typically develops from p14 onwards (Stahl et al., 2010). The number of IBA1<sup>+</sup> cells increased extensively in the VO of the GCL + IPL at p17 compared to p12. Surprisingly, we identified almost no IBA1<sup>+</sup> cells in the OPL of the VO at p17 indicating a migration of IBA1<sup>+</sup> cells from the outer towards the inner retina. The maximum of IBA1<sup>+</sup> cell density at p17 was observed in the inner retina in areas of RNV while it remained similar in the outer retina underneath RNV compared to the periphery. Again, only a few IBA1<sup>+</sup>Tom<sup>-</sup> cells (6.2  $\pm$  4.0%) were apparent in the diseased retina at p17 and were mainly restricted to areas of RNV in the GCL + IPL (Figure 2b,c). This finding was confirmed by flow cytometry analysis of the retina at p17, demonstrating that 96.1% ( $\pm$  3.7%) of CD45<sup>lo</sup>CD11b<sup>+</sup>Ly6C<sup>-</sup>Ly6G<sup>-</sup> cells were Tom<sup>+</sup> and only 3.9% ( $\pm$  3.7%) Tom<sup>-</sup> (Figure 2d). Flow cytometry analysis of peripheral blood confirmed that only negligible numbers of CD45<sup>hi</sup>CD11b<sup>+</sup>CD115<sup>+</sup>SSc<sup>lo</sup> circulating monocytes expressed the tdTomato signal in the OIR model at p10, p12, and p17 (p10: 4.7  $\pm$  4.0%, p12: 4.1  $\pm$  3.9%, p17: 0.5  $\pm$  0.7%, Figure 2e). These findings are consistent with the blood FACS results of the nOIR control group (see Figure 1g) and indicate that the OIR model itself has no significant effect on the turnover rate of peripheral blood monocytes.

Thus, our data indicate that IBA1<sup>+</sup>Tom<sup>+</sup> resident MG constitute the predominant myeloid cell population accumulating in areas of retinal ischemia and neovascularization while IBA1<sup>+</sup>Tom<sup>-</sup> blood-derived infiltrating M $\phi$  are only detectable in small numbers.

**FIGURE 1** Characterization of the *Cx3cr1<sup>CreERT2</sup>;Rosa26-tdTomato* line in the retina of young mice. (a) Experimental setup and timeline for inducing recombination (injection of tamoxifen [TAM] or solvent [sham]) and for subsequent analysis in *Cx3cr1<sup>CreERT2</sup>;Rosa26-tdTomato* mice. Breeding scheme of *Cx3cr1<sup>CreERT2</sup>* mice containing the targeted *Cx3cr1* locus with *Rosa26-tdTomato* indicator mice. Flow cytometry and immunofluorescence analysis were performed at postnatal day (p) 7, p10, p12, and p17, respectively. (b) Direct fluorescence microscopic visualization of retinal vessels (Collagen IV (COL4) staining, blue) and microglia (IBA1, green) at p17 following TAM (top) or sham (bottom) injection. TAM injection at p1 leads to an efficient tdTomato (Tom, red) labeling of most microglia. In contrast, sham-treated animals exhibit a low CreER recombination efficiency and tdTomato expression in IBA1<sup>+</sup> cells. Arrows point to IBA1<sup>+</sup> and Tom<sup>+</sup> microglia which is magnified in the top right corner of each image. OPL = outer plexiform layer. (c, d) Flow cytometry analysis of recombination efficacy in resident retinal microglia (c) and monocytes (d) in *Cx3cr1<sup>CreERT2</sup>;Rosa26-tdTomato* mice. Retinal microglia were gated and isolated as a CD45<sup>lo</sup>CD11b<sup>+</sup>Ly6C<sup>-</sup>Ly6G<sup>-</sup> cell population from the retina. Monocytes were isolated and gated as a CD45<sup>hi</sup>CD11b<sup>+</sup>CD115<sup>+</sup>SSc<sup>lo</sup> cell population from peripheral blood. Both retinal and blood myeloid cells were analyzed for their percentages of Tom<sup>+</sup> cells. Parameters of cell population were defined by fluorescence light units or scattered light units: FSC = forward scatter; SSC = sideward scatter. (e) Immunofluorescence quantification of tdTomato expression in IBA1<sup>+</sup> microglia of TAM- or sham-treated *Cx3cr1<sup>CreERT2</sup>;Rosa26-tdTomato* mice at p7, p10, p12, and p17. Sham group *n* = 17, TAM group *n* = 20. (f, g) Flow cytometric quantification of the number of tdTomato-expressing microglia in the retina (f) and monocytes in the blood (g). Data are expressed as mean  $\pm$  SD. For the analysis of the retina two mice were analyzed after sham injection and 19 mice after TAM injection. For blood analysis sham group *n* = 17, TAM group *n* = 24

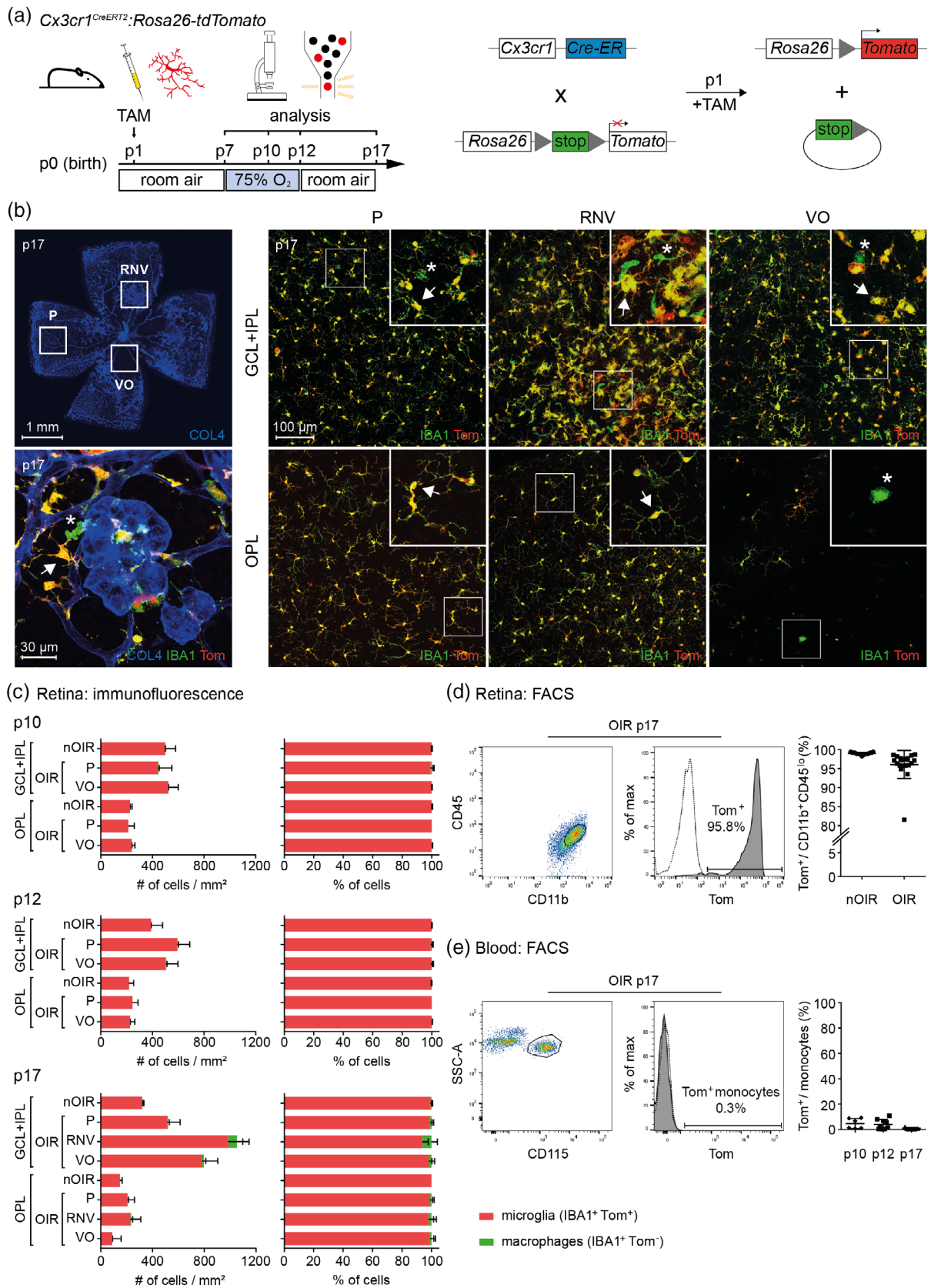


**FIGURE 2** Legend on next page.



### 3.3 | Retinal microglia proliferate in areas of ischemia and RNV

Since the low numbers of infiltrating peripheral M $\phi$  cannot account for the two- to threefold increase in myeloid cells in the diseased retina, we next explored the proliferative capacity of retinal MG in the ischemic and neovascular retina. For this purpose, we treated tamoxifen-induced *Cx3cr1<sup>CreERT2</sup>;Rosa26-tdTomato* mice with daily intraperitoneal injections of the proliferation marker EdU from p12 to p16 following OIR incubation and assessed the number of proliferating EdU<sup>+</sup>Tom<sup>+</sup> MG in the peripheral retina as well as in areas of retinal ischemia and neovascularization at p17 (Figure 3a,b).

Besides many Tom<sup>-</sup>EdU<sup>+</sup> cells that were most likely proliferating endothelial cells, pericytes or astrocytes (Bucher, Stahl, Agostini, & Martin, 2013), we detected several Tom<sup>+</sup>EdU<sup>+</sup> MG in all three areas of interest. Quantification of the absolute and relative numbers of Tom<sup>+</sup>EdU<sup>+</sup> MG revealed that overall 21.5% ( $\pm$  1.6%) of retinal MG (Tom<sup>+</sup> cells) were EdU<sup>+</sup> indicating a local microglia cell expansion from p12 to p17 in the diseased retina. Interestingly, the majority of EdU<sup>+</sup> MG were located within the inner retina (23.6  $\pm$  1.9%) compared to the outer retina (13.0  $\pm$  2.7%,  $p$  < .01) and located in areas of RNV (348.1  $\pm$  91.5 cells/mm<sup>2</sup>, 29.9  $\pm$  3.7%) compared to the VO (105.4  $\pm$  54.6 cells/mm<sup>2</sup>, 13.9  $\pm$  5.5%) and peripheral retina (145.6  $\pm$  36.6 cells/mm<sup>2</sup>, 22.9  $\pm$  4.8%, Figure 3c,d).

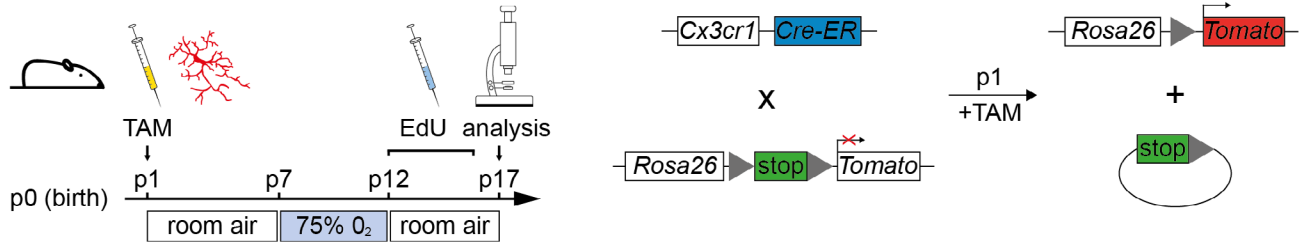
These observations demonstrate that the accumulation and increase in retinal MG in areas of retinal ischemia and neovascularization are at least partially attributable to local MG proliferation.

### 3.4 | Transcriptional profiling of retinal microglia in the OIR mouse model

Having established the quantitative changes in retinal myeloid cells, we next explored qualitative functional changes in retinal MG in

the OIR model. For this purpose, we isolated Tom<sup>+</sup> retinal MG from tamoxifen-induced *Cx3cr1<sup>CreERT2</sup>;Rosa26-tdTomato* mice at p17 following OIR incubation and performed high-throughput next-generation RNA Seq for transcriptional analysis. Tom<sup>+</sup> MG from the retina of tamoxifen-induced *Cx3cr1<sup>CreERT2</sup>;Rosa26-tdTomato* mice without OIR incubation served as controls (Figure 4a). The number of retinal MG isolated per experimental sample was similar in the OIR (9,461  $\pm$  1,846 microglia cells) and nOIR groups (8,925  $\pm$  2,371 microglia cells,  $p$  = .82), thus allowing for direct comparisons. All samples revealed high expression of MG cell markers (including *Cx3cr1*, *Hexb*, *Tmem119*, *Trem2*) and very low expression of neuronal (*Thy1*, *Isl1*, *Gabra1*, *Map2*), astrocytic (*Gfap*, *S100b*, *Tnc*), and granulocytic (*Mpo*, *S100a9*) markers, confirming the purity of our isolation procedure (Gautier et al., 2012; Greenhalgh & David, 2014; Mildner et al., 2007; Yang, Zhang, Yu, Yang, & Wang, 2014) (Figure S2). While *Tmem119* and *Hexb* expression were substantially reduced in OIR MG compared to nOIR MG, as confirmed by TMEM119 immunohistochemistry, *Cx3cr1* and *Trem2* expression in MG was stable in OIR compared to nOIR condition (Figure S3). When applying strict thresholds, a total of 304 DEG were detectable in MG in the OIR model compared to controls. Of those genes, 261 genes were significantly upregulated and 43 genes downregulated in OIR MG compared to controls (Figure 4b,c). The five most prominent DEG increased in MG in the OIR model according to the log2FC value included the *inhibitor of kappaB kinase epsilon* (*Ikbke*, log2FC = 3.0,  $p$  = 1.2E<sup>-24</sup>), *heme oxygenase 1* (*Hmox1*, log2FC = 2.6,  $p$  = 2.2E<sup>-20</sup>), *lectin, galactose binding soluble 3* (*Lgals3*, log2FC = 2.4,  $p$  = 3.3E<sup>-16</sup>), *shogushin 2a* (*Sgo2a*, log2FC = 2.4,  $p$  = 1.6E<sup>-15</sup>), and *cyclin B1* (*Ccnb1*, log2FC = 2.3,  $p$  = 1.8E<sup>-18</sup>, Figure 4c). Of note, pro-angiogenic factors such as *Ang2*, *Epo*, *Nrp1*, *Pgf* or *Vegf-a*, which are important mediators in RNV development were not significantly increased in OIR MG compared to control MG (Figure S2). To confirm our gene expression results on protein level, we quantified the protein expression of nine selected and disease-relevant DEG in

**FIGURE 2** Temporospatial distribution of myeloid subsets during retinal ischemia and neovascularization. (a) Experimental setup. Tamoxifen (TAM) was applied to 1-day-old *Cx3cr1<sup>CreERT2</sup>;Rosa26-tdTomato* mice leading to excision of the stop sequence followed by robust tdTomato (Tom) expression in microglia. Together with their dam, pups were kept in an oxygen supply chamber at 75  $\pm$  3% O<sub>2</sub> from postnatal day (p) 7 to p12 and returned to room air at p12 (OIR). Flow cytometry and immunofluorescence analysis were performed at p7, p10, p12, and p17, respectively. (b) Left above: Retinal flat-mount stained for Collagen IV (COL4) demonstrating areas of retinal neovascularization (RNV), ischemia (VO = vaso-obliterative zone) and normal peripheral vasculature (P) at p17 following OIR. Left: Higher magnification image showing retinal microglia (defined as IBA1<sup>+</sup>Tom<sup>+</sup>) and infiltrating blood-derived M $\phi$  (defined as IBA1<sup>+</sup>Tom<sup>-</sup>) surrounding a neovascular tuft stained for COL4. Right: Higher magnification images focusing on the distribution of retinal microglia (defined as IBA1<sup>+</sup>Tom<sup>+</sup>) and infiltrating blood-derived M $\phi$  (defined as IBA1<sup>+</sup>Tom<sup>-</sup>) in the ganglion cell plus inner plexiform layer (GCL + IPL, above) and outer plexiform layer (OPL, below) in areas of unaffected vasculature (P), retinal neovascularization (RNV) and ischemia (VO). Pictures are representative of six mice analyzed in two independent experiments. Arrows point to IBA1<sup>+</sup>Tom<sup>+</sup> microglia and asterisks indicate IBA1<sup>+</sup>Tom<sup>-</sup> blood-derived macrophages which are magnified in the top right corner of each image. (c) Absolute numbers (left) and the percentage (right) of myeloid subsets in the ischemic (VO), neovascular (RNV) and peripheral (P) retina at p10 (top), p12 (middle), and p17 (bottom) were analyzed following OIR. Red columns represent IBA1<sup>+</sup>Tom<sup>+</sup> microglia in *Cx3cr1<sup>CreERT2</sup>;Rosa26-tdTomato* mice whereas green columns represent blood-derived IBA1<sup>+</sup>Tom<sup>-</sup> macrophages. Data represent mean  $\pm$  SD.  $N$  = 6 (p10), 10 (p12), and 6 (p17) mice per group. (d) Flow cytometric quantification of the number of tdTomato-expressing microglia in the retina at p17 following OIR compared to untreated control mice (nOIR). Data represent means  $\pm$  SD.  $N$  = 19 (nOIR) and 20 mice (OIR). (e) Flow cytometric quantification of the number of tdTomato-expressing monocytes in the blood at p10, p12, and p17 following OIR. Data are expressed as mean  $\pm$  SD.  $N$  = 6 (p10), 9 (p12), and 9 mice (p17)

(a) *Cx3cr1<sup>CreERT2</sup>:Rosa26-tdTomato*

## Retina p17: immunofluorescence

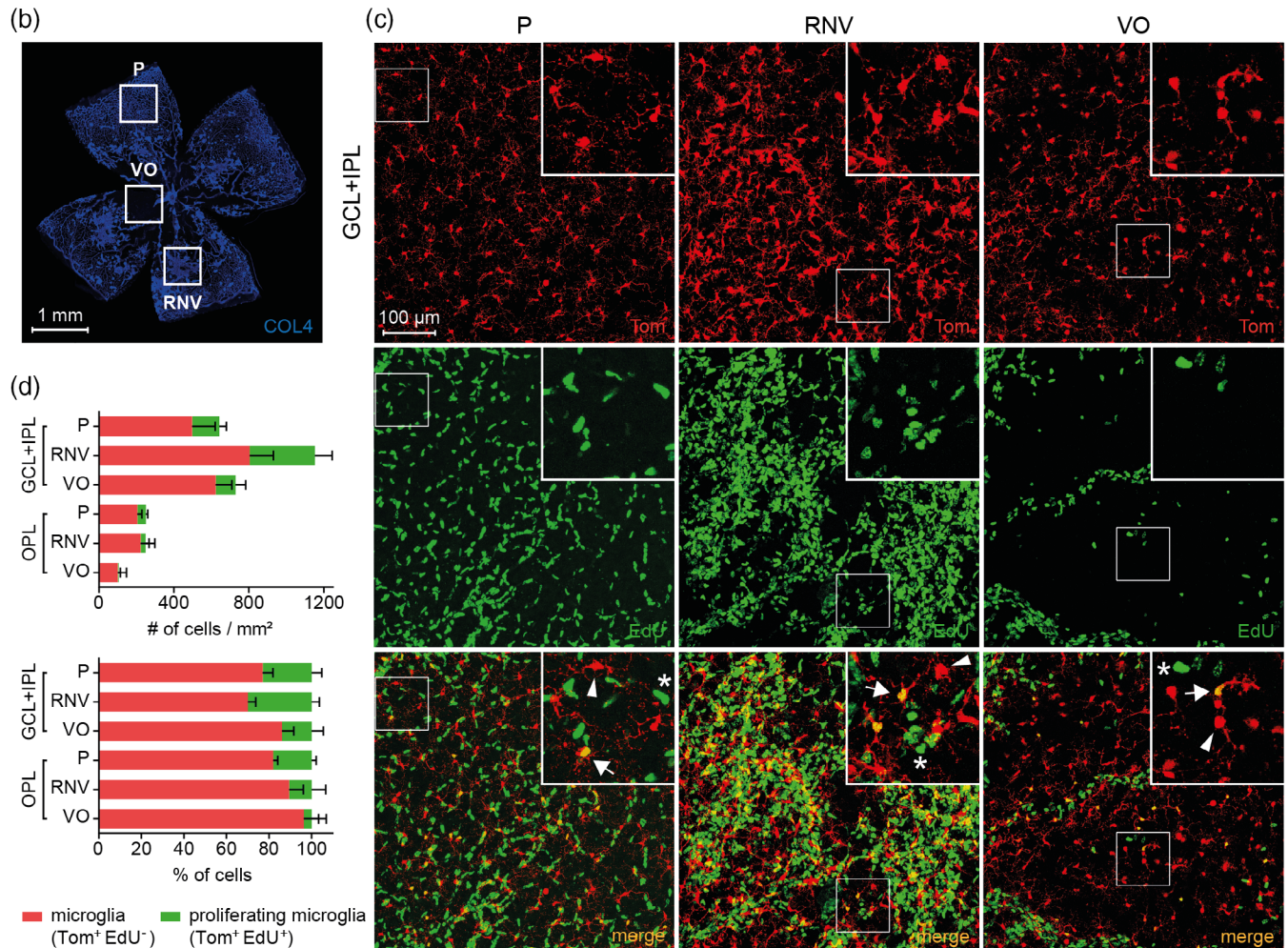
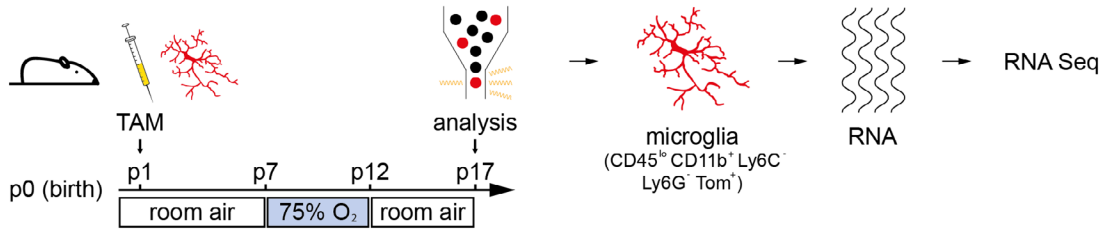


**FIGURE 3** Retinal microglia proliferate in areas of retinal ischemia and neovascularization. (a) Experimental setup. Tamoxifen (TAM) was applied to 1-day-old *Cx3cr1<sup>CreERT2</sup>:Rosa26-tdTomato* mice leading to robust tdTomato (Tom) expression in microglia. Pups were kept at 75 ± 3% O<sub>2</sub> from postnatal day (p) 7 to p12 and returned to room air (OIR). Pups received a daily intraperitoneal injection of 5-ethynyl-2'-deoxyuridine (EdU) from p12 to p16 and were sacrificed at p17 for immunofluorescence analysis. (b) Retinal flat-mount stained for Collagen IV (COL4) demonstrating areas of retinal neovascularization (RNV), ischemia (VO = vaso-obliterative zone) and normal peripheral vasculature (P) at p17 following OIR incubation. (c) Higher magnification images focusing on the distribution of retinal microglia (Tom<sup>+</sup>, red) that have undergone mitosis (EdU<sup>+</sup>, green) in the ganglion cell plus inner plexiform layer (GCL + IPL) in areas of normal peripheral vasculature (P), RNV and VO. Arrows point to retinal microglia (Tom<sup>+</sup>, red) which have undergone proliferation (Tom<sup>+</sup>EdU<sup>+</sup>, yellow), arrowheads point to retinal microglia which have not undergone proliferation (Tom<sup>+</sup>EdU<sup>-</sup>, red) and asterisks illustrate nonmicroglial cells that have proliferated (Tom<sup>-</sup>EdU<sup>+</sup>, green). Higher magnification images in the top right corner. Pictures are representative of five mice analyzed in one experiment. (d) Absolute numbers (top) and percentages (bottom) of microglia with or without EdU signal in areas of P, VO, and RNV at p17 following OIR. Columns represent nonproliferating (red) and proliferating microglia (green) respectively. Data represent means ± SD. N = 5 per group

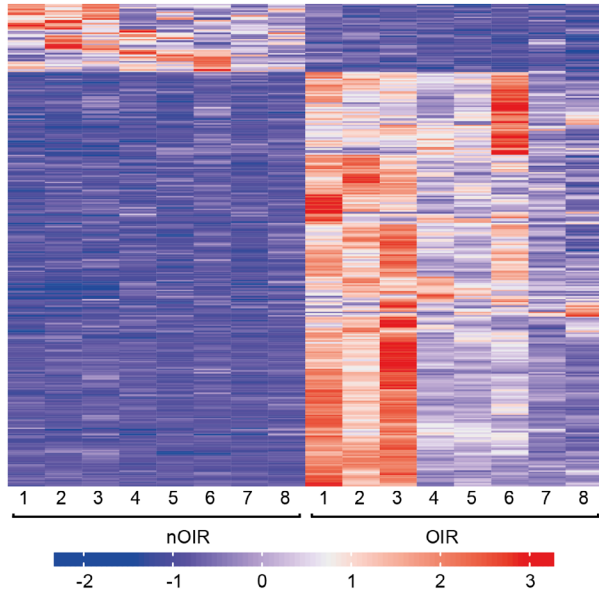




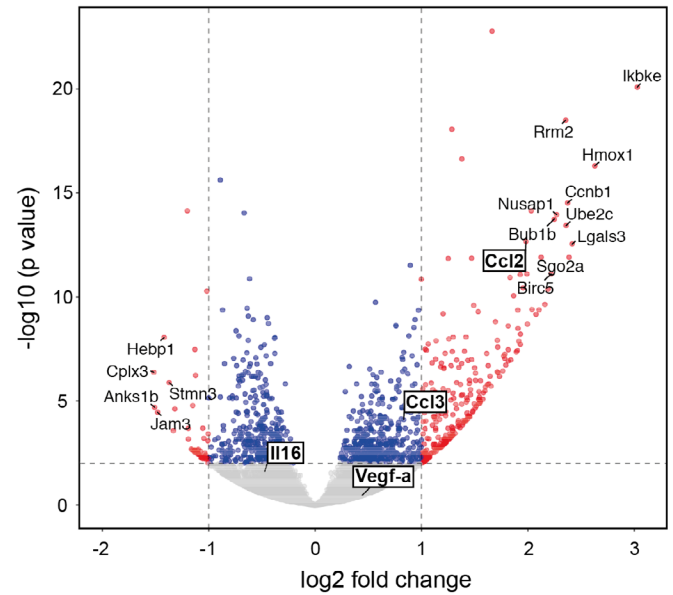
(a) *Cx3cr1<sup>CreERT2</sup>; Rosa26-tdTomato*



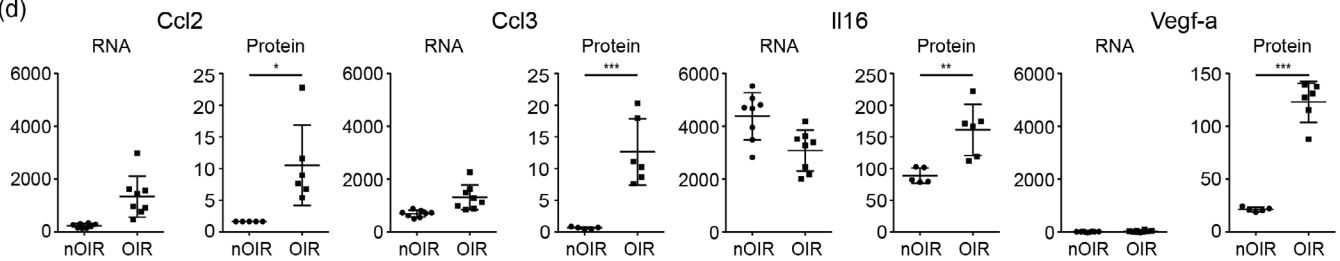
(b)



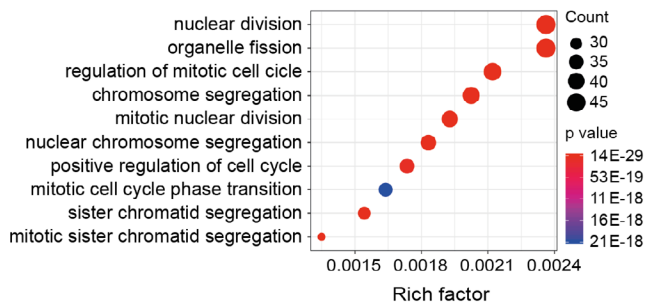
(c)



(d)



(e) GO term enrichment - Biological Processes



(f) GO term enrichment - Molecular Function

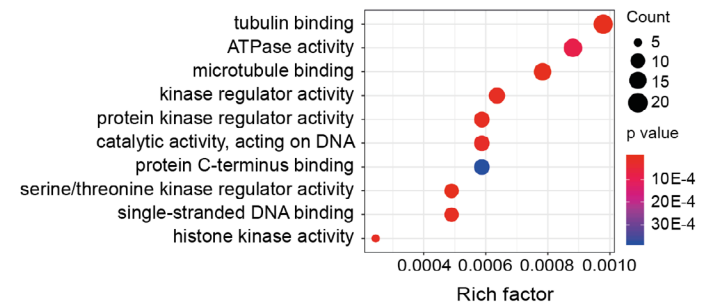


FIGURE 4 Legend on next page.

the retina of OIR and control mice that were analyzable using a commercially available multiplex protein analysis platform. The chemokines CCL2 (OIR:  $10.5 \pm 6.3$  pg/ml, nOIR:  $1.6 \pm 0$  pg/ml,  $p < .05$ ), CCL3 (OIR:  $12.6 \pm 5.2$  pg/ml, nOIR:  $0.7 \pm 0.2$  pg/ml,  $p < .005$ ) and CXCL2 (OIR:  $1.0 \pm 1.0$  pg/ml, nOIR:  $0.1 \pm 0$  pg/ml,  $p = .08$ ) were increased in the OIR group retinas compared to controls which recapitulates our RNA Seq analysis findings. In contrast to their concentration in MG on RNA level, IL16 (OIR:  $160.9 \pm 40.4$  pg/ml, nOIR:  $88.9 \pm 12$  pg/ml) and VEGF (OIR:  $123.1 \pm 19.3$  pg/ml, nOIR:  $21.4 \pm 2.2$  pg/ml,  $p < .05$ ) which served as a positive control (Clemens Lange et al., 2016) were significantly increased in the OIR retina compared to controls (Figure 4d). The corresponding protein concentrations of the DEG *Ccl4*, *Il1b*, *Il6*, and *Tnfa* were below the detection rate and not recorded (data not shown).

To further investigate the biological importance of the DEG, we performed GO enrichment analysis. The GO enrichment analysis revealed that numerous DEGs were involved in a variety of biological processes, such as nuclear division (GO:0000280,  $p = 4.4E^{-32}$ ), organelle fission (GO:0048285,  $p = 6.9E^{-30}$ ), regulation of the mitotic cell cycle (GO:0000280,  $p = 1.5E^{-23}$ ), chromosome segregation (GO:0007059,  $p = 4.7E^{-30}$ ) and mitotic nuclear division (GO:0140014,  $p = 4.4E^{-30}$ ) supporting the observation of increased MG cell expansion in the OIR model (Figure 4e). Molecular function GO enrichment analysis showed that the upregulated genes were mainly involved in tubulin-binding (GO:0015631,  $p = 4.1E^{-6}$ ), ATPase activity (GO:0016887,  $p = 1.7E^{-5}$ ), microtubule-binding (GO:0008017,  $p = 1.1E^{-7}$ ), and kinase and protein kinase regulatory activity (GO:0019207,  $p = 1.6E^{-6}$ ; GO:0019887,  $p = 1.5E^{-6}$ , Figure 4f). Furthermore, GO clusters related to chemokine signaling such as chemokine activity (GO: 0008009,  $p = .002$ ), CCR chemokine receptor binding (GO:0048020,  $p = .003$ ) and cytokine receptor binding (GO:0005126,  $p = .004$ ) were significantly enriched in retinal microglia in the OIR model. To visualize functionally enriched GO clusters, we used cnetplots depicting the linkages of genes and biological concepts as a network (Figure S4).

## 4 | DISCUSSION

### 4.1 | *Cx3cr1<sup>CreERT2</sup>:Rosa26-tdTomato* mice are a suitable tool to investigate the role of retinal microglia in the OIR mouse model

Our knowledge on retinal myeloid cell dynamics and turnover in health and ischemic retinal disease is based on transplantation experiments, where bone marrow from ubiquitously expressing green fluorescent protein transgenic mice, for example, those driven by the  $\beta$ -Actin promoter, was transplanted into irradiated wildtype recipients (Kataoka et al., 2011). To exclude confounding variables such as transplantation efficacy and irradiation-induced breakdown of the blood-retinal barrier which clearly biased turnover experiments in the past (Kezic & McMenamin, 2013), we used a distinct strategy in *Cx3cr1<sup>CreERT2</sup>:Rosa26-tdTomato* mice to differentially investigate the turnover and expansion of resident microglia cells and blood-derived recruited myeloid cells in health and in a model for neovascular retinal disease. We observed that a tamoxifen pulse treatment of newborn *Cx3cr1<sup>CreERT2</sup>:Rosa26-tdTomato* mice led to almost complete and persistent labeling of retinal MG, whereas the *tdTomato* labeling of circulating *Cx3cr1*-expressing cells quickly subsided within 2 weeks. This observation follows the findings of Goldmann et al. in adult *Cx3cr1<sup>CreERT2</sup>* mice crossed to a floxed *Rosa26*-dependent reporter line (*YFP*) and can be explained by the rapid cell turnover of bone marrow-derived blood monocytes in contrast to the low turnover rate of MG (Goldmann et al., 2013; Wieghofer et al. 2015). Interestingly, sham-injected newborn *Cx3cr1<sup>CreERT2</sup>:Rosa26-tdTomato* mice also revealed *tdTomato* expression in about 20% of retinal MG, which increased over time, but not in circulating monocytes. These data indicate an accumulation of spontaneous and tamoxifen-independent CreER-mediated recombination events in the *Rosa26* locus of *Cx3cr1<sup>CreERT2</sup>:Rosa26-tdTomato* mice, and was reported previously in brain MG (Weber et al., 2018). While that observation does not affect the present study, it needs to be considered when working with *Cx3cr1<sup>CreERT2</sup>:Rosa26-tdTomato* mice, especially when conducting time- and CreER/loxP-dependent conditional knockout experiments.

**FIGURE 4** Transcriptional alterations of retinal microglia in the context of retinal ischemia and neovascularization. (a) Experimental setup.  $CD45^{\text{lo}}CD11b^+Ly6C^-Ly6G^+Tom^+$  microglia of tamoxifen- and OIR-treated *Cx3cr1<sup>CreERT2</sup>:Rosa26-tdTomato* mice were isolated at postnatal day (p) 17 using flow cytometry-based cell sorting and processed for RNA Seq and protein analysis. (b) Supervised heatmap clustering of the 304 differentially expressed genes ( $\leq 0.01$  and  $\log_2FC \geq 1$ ) in microglia in control (nOIR) and OIR mice.  $N = 8$  samples per group. (c) Volcano plot displaying differentially expressed genes in retinal microglia in OIR and nOIR control tissues. The vertical axis (y-axis) corresponds to the mean expression value of  $-\log_{10} p$ -value, and the horizontal axis (x-axis) displays the  $\log_2$  fold change value. The top 10 upregulated and top 5 downregulated expressed transcripts are labeled. Positive x-values represent upregulation and negative x-values represent downregulation. (d) Comparison of RNA Seq results of isolated microglia and protein analysis of retinal tissue lysates under OIR and nOIR control condition focusing on relevant and differentially expressed factors. mRNA levels are expressed as transcripts per million, protein levels as pg/ $\mu$ l. mRNA:  $n = 8$  samples per group, protein  $n = 5-6$  animals per group. (e, f) Gene ontology (GO) enrichment analyses for the 304 differentially expressed genes. Dot plot depicting the top 10 enriched GO terms with the largest gene ratios for biological processes (e) and molecular function (f) in order of gene ratio. The size of the dots represents the number of genes in the significant differentially expressed gene list associated with the GO term, and dots' colors represent the  $p$ -adjusted values



## 4.2 | Origin of retinal myeloid cells in health and during OIR

Having established that *Cx3cr1<sup>CreERT2</sup>;Rosa26-tdTomato* mice are suitable to selectively study microglia biology in young mice, we next investigated the temporospatial distribution of resident MG and recruited blood-derived M $\phi$  in *Cx3cr1<sup>CreERT2</sup>;Rosa26-tdTomato* mice in the steady state and in a mouse model for retinal ischemia and neovascularization, the OIR model. Under homeostatic conditions, almost all IBA1<sup>+</sup> retinal myeloid cells were Tom<sup>+</sup> MG and no blood-derived infiltrating M $\phi$  (defined as IBA1<sup>+</sup>Tom<sup>-</sup>) were detected in the retina. These findings concur with the prevailing notion of a stable retinal microglia cell population that is not complemented by circulating monocytes in the steady state (O'Koren, Mathew, & Saban, 2016). Next, we assessed the number of IBA1<sup>+</sup> myeloid cells in the retina over the course of the OIR model and detected a substantial increase of myeloid cells in the vascularized periphery and VO starting between p10 and p12 as well as in areas of RNV at p17, a finding in line with earlier reports (Davies, Eubanks, & Powers, 2006; Dejda et al., 2014; Liyanage et al., 2016). The overall increase in myeloid cells in the OIR model raises the question of the origin of these cells. In contrast to the prevailing notion of a major influx of blood-derived myeloid cells into the diseased retina (Dejda et al., 2014; Kataoka et al., 2011), our data strongly suggest that resident MG constitute the predominant myeloid cell population in areas of retinal ischemia and neovascularization whereas blood-derived M $\phi$  play a negligible role in terms of quantity. Kataoka and colleagues analyzed lethally irradiated bone marrow-reconstituted mice and reported on a considerable number of bone-marrow-derived cells accumulating in the retina, in particular in areas of RNV in the OIR model (Kataoka et al., 2011). Although head shielding was used to suppress irradiation-induced tissue damage and cytokine release attracting myeloid cells in this study (Kierdorf, Katzmarski, Haas, & Prinz, 2013), the presence of bone marrow in the bloodstream of young mice paired with (sub-) lethal irradiation of the entire body early during development is likely to exert secondary long-lasting systemic effects during postnatal development and may have affected the results (Ajami, Bennett, Krieger, Tetzlaff, & Rossi, 2007; Shemer et al., 2018). Dejda and colleagues demonstrated a proportional increase in Neuropilin1<sup>+</sup> mononuclear phagocytes in the OIR model, with a 155% rise at p17, and postulated that this subpopulation was being recruited from the blood during disease. The flow cytometric gating strategy used in their study, which excluded Gr-1<sup>+</sup> peripheral cells like monocytes, and neutrophils, however, makes it difficult to discriminate resident MG and infiltrating blood-derived M $\phi$  with confidence (Dejda et al., 2014). In addition, the usage of the *Lyz2-Cre* mouse model, which predominantly targets peripheral myeloid cells and to a lesser extent MG, is likely to lead to mixed Neuropilin1<sup>+</sup> and Neuropilin1<sup>-</sup> populations in both, resident MG and peripheral myeloid cells (Goldmann et al., 2013; Wieghofer et al. 2015). Of note, our RNA Seq data revealed strong RNA expression of *Neuropilin1* in retinal MG, indicating that the increase in Neuropilin1<sup>+</sup> mononuclear phagocytes observed by Dejda et al. is compatible with a local proliferation of resident MG in

the OIR model. Furthermore, our study demonstrates that retinal MG has a considerable capacity to proliferate in areas of retinal ischemia and neovascularization. This finding concurs with previous studies in the brain (Ladeby et al., 2005) but challenges earlier reports of low proliferation of resident MG in the diseased OIR retina (Davies et al., 2006; Dejda et al., 2014). However, in these studies, MG identification was limited by the lack of a cell-specific marker or a suitable *in vivo* model and was solely based on immunohistochemistry or FACS analysis of Gr-1<sup>-</sup>F4/80<sup>+</sup>CD11b<sup>+</sup> mononuclear phagocytes. Furthermore, in contrast to our study, Bromodeoxyuridine was applied only once after oxygen exposure, 24 hr before sacrifice, whereas our study documents the cumulative MG proliferation capacity from p12 to p17. It is, therefore, possible that previous studies have underestimated the proliferative capacity of MG in the OIR model. However, as only every fifth retinal microglia cell had undergone division in our study by postnatal day 17, proliferation alone seems insufficient to account for the increased microglia cell number in the neovascular zone. This is also suggested by the notion that only a small fraction of MG undergoes more than one cell division cycle and that even fewer cells proliferate repeatedly under diseased conditions (Tay, Mai, Dautzenberg, Fernández-Klett, & Lin, 2017). Our finding that the number of retinal MG decreases in the outer plexiform layer at p12 and is practically absent in the VO at p17 suggests a vertical migration of retinal MG to the inner retina's site of injury. It is also possible that a fraction of the accreting retinal MG originates from extraretinal central nervous system areas and that they migrate from the optic nerve or ciliary body and iris to the damaged retina as recently described (Huang et al., 2018). Taken together, these observations strongly suggest a local proliferation and migratory redistribution of MG in areas of retinal ischemia and neovascularization which may be complemented by an influx of Tom<sup>+</sup> myeloid cells from the optic nerve or ciliary body (Huang et al., 2018).

## 4.3 | Transcriptional profiling of retinal microglia during OIR

Previous studies have indicated that the depletion of mononuclear phagocytes results in a reduction of pathological neovascularization in the OIR model (Kataoka et al., 2011) and that MG induce angiogenesis by expressing pro-angiogenic and inflammatory cytokines (Ding et al., 2018). Unfortunately, comprehensive transcriptional analyses of retinal MG during retinal ischemia and neovascularization have not been available. To address this issue and further unravel molecular functions and biological processes in retinal MG in the context of retinal ischemia and neovascularization, we isolated retinal MG at the peak of RNV (p17) in the OIR model and performed high-throughput RNA Seq. Our results demonstrate considerable differences in mRNA expression between activated retinal MG in the OIR model compared to quiescent microglia in the steady state. Activated retinal MG in the OIR model showed downregulation of MG signature genes such as *Tmem119* and *Hexb*, which is consistent with previous studies showing reduced expression of TMEM119 in activated retinal MG in mouse models of

neovascular and degenerative diseases (O'Koren et al., 2019; Su et al., 2019). GO cluster analysis revealed that processes related to cell division were significantly upregulated in retinal MG during OIR, supporting our immunohistochemical findings of local microglia cell expansion. Among them, *Igf1*, *Mif*, *Ccnb2*, and *Cdk1* which are known to be essential for microglia cell proliferation in the central nervous system (Arnò et al., 2014; O'Donnell, Frederick, Krady, Vannucci, & Wood, 2002; Pepe et al., 2017). Furthermore, factors belonging to GO clusters related to chemokine signaling, including *Ccl2*, *Ccl3*, *Ccl4*, *Ccl7*, *Nes*, and *Cxcl14* were upregulated in MG in the OIR model, emphasizing the involvement of these factors during microglia cell activation and migration into the diseased retina. In contrast to the pro-angiogenic role of retinal MG in neovascular eye disease postulated in the literature, we did not observe upregulated pro-angiogenic factors in MG such as *Epo*, *Pgf*, *Ang2*, or *Vegf* which are important mediators for the development of RNV. In particular, the expression of *Vegf* in retinal MG was negligible, confirming previous findings (Liyanage et al., 2016) and indicating that retinal MG is neither a major source of VEGF in the ischemic retina, nor do they contribute to development of RNV by expressing VEGF. Of note, the results of this study are limited due to the use of bulk RNA Seq, which averages the expression levels of thousands of MG and may, therefore, fail to detect subtle but biologically meaningful differences between different MG subpopulations in the diseased retina. This is particularly important in light of the identification of distinct disease-associated MG in the brain, which represents a subpopulation contributing to neurodegenerative brain disease (Keren-Shaul et al., 2017). Future studies using single-cell RNA Seq are therefore warranted to determine the precise role of different retinal MG populations during the development of ischemia-induced RNV.

In summary, this study demonstrates that *Cx3cr1<sup>CreERT2</sup>; Rosa26-tdTomato* mice are highly valuable to assess microglia cell biology in young mice in the OIR mouse model. In contrast to the prevailing notion, we found that resident MG do indeed proliferate, and that they constitute the predominant myeloid cell population in areas of retinal ischemia and neovascularization whereas blood-derived M $\phi$  play a minor role in terms of quantity. On the transcriptional level, retinal MG revealed a proliferating and migratory phenotype in the OIR model with an upregulation of diverse pro-inflammatory cytokines which may contribute to ischemic neovascular eye disease. The intracellular pathways unraveled in this study provide a basis for future studies aiming to modulate retinal MG in ischemic neovascular eye disease.

## ACKNOWLEDGMENTS

The authors thank Gabriele Prinz, Marc Guder, Johannes Baumann, and Omar Mossad for excellent technical assistance; M. Follo and team at lighthouse fluorescence technologies core facility, University Medical Center, Freiburg for cell sorting; CEMT, University of Freiburg for excellent animal care; KFB, Center of Excellence for Fluorescent Bioanalytics, Regensburg for RNA Seq analysis; Marco Prinz for providing *Cx3cr1<sup>CreERT2</sup>; Rosa26-tdTomato* mice. This study was supported by the Else-Kröner-Fresenius Stiftung and the Deutsche Forschungsgemeinschaft (SFB/TRR167).

## CONFLICT OF INTEREST

The authors declare no conflict of interest.

## DATA AVAILABILITY STATEMENT

The data that support the findings of this study are available from the corresponding author upon reasonable request.

## ORCID

Marco Prinz  <https://orcid.org/0000-0002-0349-1955>

Clemens Lange  <https://orcid.org/0000-0002-2580-6823>

## REFERENCES

- Afgan, E., Baker, D., van den Beek, M., Blankenberg, D., Bouvier, D., Cech, M., ... Goecks, J. (2016). The galaxy platform for accessible, reproducible and collaborative biomedical analyses: 2016 update. *Nucleic Acids Research*, 44(W1), W3–W10. <https://doi.org/10.1093/nar/gkw343>
- Ajami, B., Bennett, J. L., Krieger, C., Tetzlaff, W., & Rossi, F. M. V. (2007). Local self-renewal can sustain CNS microglia maintenance and function throughout adult life. *Nature Neuroscience*, 10(12), 1538–1543. <https://doi.org/10.1038/nn2014>
- Andrews, S. (2018). *FastQC A Quality Control tool for High Throughput Sequence Data*. <http://www.bioinformatics.babraham.ac.uk/projects/fastqc/>
- Arnò, B., Grassivaro, F., Rossi, C., Bergamaschi, A., Castiglioni, V., Furlan, R., ... Muzio, L. (2014). Neural progenitor cells orchestrate microglia migration and positioning into the developing cortex. *Nature Communications*, 5, 5611. <https://doi.org/10.1038/ncomms6611>
- Bucher, F., Stahl, A., Agostini, H. T., & Martin, G. (2013). Hyperoxia causes reduced density of retinal astrocytes in the central avascular zone in the mouse model of oxygen-induced retinopathy. *Molecular and Cellular Neurosciences*, 56, 225–233. <https://doi.org/10.1016/j.mcn.2013.06.001>
- Davies, M. H., Eubanks, J. P., & Powers, M. R. (2006). Microglia and macrophages are increased in response to ischemia-induced retinopathy in the mouse retina. *Molecular Vision*, 12, 467–477.
- Dejda, A., Mawambo, G., Cerani, A., Miloudi, K., Shao, Z., Daudelin, J.-F., ... Sapieha, P. (2014). Neuropilin-1 mediates myeloid cell chemoattraction and influences retinal neuroimmune crosstalk. *The Journal of Clinical Investigation*, 124(11), 4807–4822. <https://doi.org/10.1172/JCI76492>
- Ding, X., Gu, R., Zhang, M., Ren, H., Shu, Q., Xu, G., & Wu, H. (2018). Microglia enhanced the angiogenesis, migration and proliferation of co-cultured RMECs. *BMC Ophthalmology*, 18. <https://doi.org/10.1186/s12886-018-0886-z>
- Dobin, A., Davis, C. A., Schlesinger, F., Drenkow, J., Zaleski, C., Jha, S., ... Gingeras, T. R. (2013). STAR: Ultrafast universal RNA-seq aligner. *Bioinformatics (Oxford, England)*, 29(1), 15–21. <https://doi.org/10.1093/bioinformatics/bts635>
- Figueira, J., Fletcher, E., Massin, P., Silva, R., Bandello, F., Midena, E., ... EVICR.net Study Group. (2018). Ranibizumab plus Panretinal photocoagulation versus Panretinal photocoagulation alone for high-risk proliferative diabetic retinopathy (PROTEUS study). *Ophthalmology*, 125(5), 691–700. <https://doi.org/10.1016/j.ophtha.2017.12.008>
- Gautier, E. L., Shay, T., Miller, J., Greter, M., Jakubzick, C., Ivanov, S., ... Immunological Genome Consortium. (2012). Gene-expression profiles and transcriptional regulatory pathways that underlie the identity and diversity of mouse tissue macrophages. *Nature Immunology*, 13(11), 1118–1128. <https://doi.org/10.1038/ni.2419>
- Goldmann, T., Wieghofer, P., Müller, P. F., Wolf, Y., Varol, D., Yona, S., ... Prinz, M. (2013). A new type of microglia gene targeting shows TAK1





- to be pivotal in CNS autoimmune inflammation. *Nature Neuroscience*, 16(11), 1618–1626. <https://doi.org/10.1038/nn.3531>
- Green, W. R. (1991). Clinicopathologic studies of treated choroidal neovascular membranes. A review and report of two cases. *Retina*, 11, 328–356.
- Greenhalgh, A. D., & David, S. (2014). Differences in the phagocytic response of microglia and peripheral macrophages after spinal cord injury and its effects on cell death. *The Journal of Neuroscience: The Official Journal of the Society for Neuroscience*, 34(18), 6316–6322. <https://doi.org/10.1523/JNEUROSCI.4912-13.2014>
- Gu, Z., Eils, R., & Schlesner, M. (2016). Complex heatmaps reveal patterns and correlations in multidimensional genomic data. *Bioinformatics (Oxford, England)*, 32(18), 2847–2849. <https://doi.org/10.1093/bioinformatics/btw313>
- Hackett, S. F., Ozaki, H., Strauss, R. W., Wahlin, K., Suri, C., Maisonpierre, P., ... Campochiaro, P. A. (2000). Angiopoietin 2 expression in the retina: Upregulation during physiologic and pathologic neovascularization. *Journal of Cellular Physiology*, 184(3), 275–284. [https://doi.org/10.1002/1097-4652\(200009\)184:3<275::AID-JCP1>3.0.CO;2-7](https://doi.org/10.1002/1097-4652(200009)184:3<275::AID-JCP1>3.0.CO;2-7)
- Huang, Y., Xu, Z., Xiong, S., Sun, F., Qin, G., Hu, G., ... Peng, B. (2018). Repopulated microglia are solely derived from the proliferation of residual microglia after acute depletion. *Nature Neuroscience*, 21(4), 530–540. <https://doi.org/10.1038/s41593-018-0090-8>
- Kataoka, K., Nishiguchi, K. M., Kaneko, H., van Rooijen, N., Kachi, S., & Terasaki, H. (2011). The roles of vitreal macrophages and circulating leukocytes in retinal neovascularization. *Investigative Ophthalmology & Visual Science*, 52(3), 1431–1438. <https://doi.org/10.1167/iovs.10-5798>
- Keren-Shaul, H., Spinrad, A., Weiner, A., Matcovitch-Natan, O., Dvir-Szternfeld, R., Ulland, T. K., ... Amit, I. (2017). A unique microglia type associated with restricting development of Alzheimer's disease. *Cell*, 169(7), 1276–1290.e17. <https://doi.org/10.1016/j.cell.2017.05.018>
- Kezic, J. M., & McMenamin, P. G. (2013). The effects of CX3CR1 deficiency and irradiation on the homing of monocyte-derived cell populations in the mouse eye. *PLoS ONE*, 8(7), e68570. <https://doi.org/10.1371/journal.pone.0068570>
- Kierdorf, K., Katzmarski, N., Haas, C. A., & Prinz, M. (2013). Bone marrow cell recruitment to the brain in the absence of irradiation or parabiosis bias. *PLoS ONE*, 8(3), e58544. <https://doi.org/10.1371/journal.pone.0058544>
- Ladeby, R., Wrenfeldt, M., Garcia-Ovejero, D., Fenger, C., Dissing-Olesen, L., Dalmau, I., & Finsen, B. (2005). Microglial cell population dynamics in the injured adult central nervous system. *Brain Research. Brain Research Reviews*, 48(2), 196–206. <https://doi.org/10.1016/j.brainresrev.2004.12.009>
- Lange, C., Ehlken, C., Stahl, A., Martin, G., Hansen, L., & Agostini, H. T. (2009). Kinetics of retinal vaso-obliteration and neovascularisation in the oxygen-induced retinopathy (OIR) mouse model. *Graefes Archive for Clinical and Experimental Ophthalmology*, 247, 1205–1211. <https://doi.org/10.1007/s00417-009-1116-4>
- Lange, C., Mowat, F., Sayed, H., Mehad, M., Duluc, L., Piper, S., ... Bainbridge, J. (2016). Dimethylarginine dimethylaminohydrolase-2 deficiency promotes vascular regeneration and attenuates pathological angiogenesis. *Experimental Eye Research*, 147, 148–155. <https://doi.org/10.1016/j.exer.2016.05.007>
- Liao, Y., Smyth, G. K., & Shi, W. (2014). featureCounts: An efficient general purpose program for assigning sequence reads to genomic features. *Bioinformatics (Oxford, England)*, 30(7), 923–930. <https://doi.org/10.1093/bioinformatics/btt656>
- Liyanage, S. E., Fantin, A., Villacampa, P., Lange, C. A., Denti, L., Cristante, E., ... Ruhrberg, C. (2016). Myeloid-derived vascular endothelial growth factor and hypoxia-inducible factor are dispensable for ocular neovascularization—Brief report. *Arteriosclerosis, Thrombosis, and Vascular Biology*, 36(1), 19–24. <https://doi.org/10.1161/ATVBAHA.115.306681>
- Love, M. I., Huber, W., & Anders, S. (2014). Moderated estimation of fold change and dispersion for RNA-seq data with DESeq2. *Genome Biology*, 15(12), 550. <https://doi.org/10.1186/s13059-014-0550-8>
- Mildner, A., Schmidt, H., Nitsche, M., Merkler, D., Hanisch, U.-K., Mack, M., ... Prinz, M. (2007). Microglia in the adult brain arise from Ly-6ChiCCR2+ monocytes only under defined host conditions. *Nature Neuroscience*, 10(12), 1544–1553. <https://doi.org/10.1038/nn2015>
- Mowat, F. M., Gonzalez, F., Luhmann, U. F. O., Lange, C. A., Duran, Y., Smith, A. J., ... Bainbridge, J. W. B. (2012). Endogenous erythropoietin protects neuroretinal function in ischemic retinopathy. *The American Journal of Pathology*, 180(4), 1726–1739. <https://doi.org/10.1016/j.ajpath.2011.12.033>
- O'Koren, E. G., Mathew, R., & Saban, D. R. (2016). Fate mapping reveals that microglia and recruited monocyte-derived macrophages are definitively distinguishable by phenotype in the retina. *Scientific Reports*, 6, 20636. <https://doi.org/10.1038/srep20636>
- O'Koren, E. G., Yu, C., Klingeborn, M., Wong, A. Y. W., Prigge, C. L., Mathew, R., ... Saban, D. R. (2019). Microglial function is distinct in different anatomical locations during retinal homeostasis and degeneration. *Immunity*, 50(3), 723–737.e7. <https://doi.org/10.1016/j.immuni.2019.02.007>
- O'Donnell, S. L., Frederick, T. J., Krady, J. K., Vannucci, S. J., & Wood, T. L. (2002). IGF-I and microglia/macrophage proliferation in the ischemic mouse brain. *GLIA*, 39(1), 85–97. <https://doi.org/10.1002/glia.10081>
- Pepe, G., De Maglie, M., Minoli, L., Villa, A., Maggi, A., & Vegeto, E. (2017). Selective proliferative response of microglia to alternative polarization signals. *Journal of Neuroinflammation*, 14(1), 236. <https://doi.org/10.1186/s12974-017-1011-6>
- Sapieha, P., Hamel, D., Shao, Z., Rivera, J. C., Zaniolo, K., Joyal, J. S., & Chemtob, S. (2010). Proliferative retinopathies: Angiogenesis that blinds. *The International Journal of Biochemistry & Cell Biology*, 42(1), 5–12. <https://doi.org/10.1016/j.biocel.2009.10.006>
- Schindelin, J., Arganda-Carreras, I., Frise, E., Kaynig, V., Longair, M., Pietzsch, T., ... Cardona, A. (2012). Fiji: An open-source platform for biological-image analysis. *Nature Methods*, 9(7), 676–682. <https://doi.org/10.1038/nmeth.2019>
- Shemer, A., Grozovski, J., Tay, T. L., Tao, J., Volaski, A., Süß, P., ... Jung, S. (2018). Engrafted parenchymal brain macrophages differ from microglia in transcriptome, chromatin landscape and response to challenge. *Nature Communications*, 9. <https://doi.org/10.1038/s41467-018-07548-5>
- Sousa, C., Biber, K., & Michelucci, A. (2017). Cellular and molecular characterization of microglia: A unique immune cell population. *Frontiers in Immunology*, 8. <https://doi.org/10.3389/fimmu.2017.00198>
- Stahl, A., Chen, J., Sapieha, P., Seaward, M. R., Krah, N. M., Dennison, R. J., ... Smith, L. E. H. (2010). Postnatal weight gain modifies severity and functional outcome of oxygen-induced proliferative retinopathy. *The American Journal of Pathology*, 177(6), 2715–2723. <https://doi.org/10.2353/ajpath.2010.100526>
- Stahl, A., Connor, K. M., Sapieha, P., Chen, J., Dennison, R. J., Krah, N. M., ... Smith, L. E. H. (2010). The mouse retina as an angiogenesis model. *Investigative Ophthalmology & Visual Science*, 51(6), 2813–2826. <https://doi.org/10.1167/iovs.10-5176>
- Stahl, A., Krohne, T. U., Eter, N., Oberacher-Velten, I., Guthoff, R., Meltendorf, S., ... Comparing Alternative Ranibizumab Dosages for Safety and Efficacy in Retinopathy of Prematurity (CARE-ROP) Study Group. (2018). Comparing alternative Ranibizumab dosages for safety and efficacy in retinopathy of prematurity: A randomized clinical trial. *JAMA Pediatrics*, 172(3), 278–286. <https://doi.org/10.1001/jamapediatrics.2017.4838>
- Su, N., März, S., Plagemann, T., Cao, J., Schnittler, H.-J., Eter, N., & Heiduschka, P. (2019). Occurrence of transmembrane protein 119 in the retina is not restricted to the microglia: An immunohistochemical study. *Translational Vision Science & Technology*, 8(6), 29–29. <https://doi.org/10.1167/tvst.8.6.29>



- Tay, T. L., Mai, D., Dautzenberg, J., Fernández-Klett, F., Lin, G., Sagar, D. M., ... Prinz, M. (2017). A new fate mapping system reveals context-dependent random or clonal expansion of microglia. *Nature Neuroscience*, *20*(6), 793–803. <https://doi.org/10.1038/nn.4547>
- Wang, X., Abraham, S., McKenzie, J. A., Jeffs, N., Swire, M., Tripathi, V. B., ... Greenwood, J. (2013). LRG1 promotes angiogenesis by modulating endothelial TGF-beta signalling. *Nature*, *499*(1476-4687 [Electronic]), 306–311. <https://doi.org/10.1038/nature12345>
- Weber, M. D., McKim, D. B., Niraula, A., Witcher, K. G., Yin, W., Sobol, C. G., ... Godbout, J. P. (2018). The influence of microglial elimination and repopulation on stress sensitization induced by repeated social defeat. *Biological Psychiatry*, *85*, 667–678. <https://doi.org/10.1016/j.biopsych.2018.10.009>
- Wieghofer, P., Knobeloch, K. P., & Prinz, M. (2015). Genetic targeting of microglia. *Glia*, *63*(1), 1–22. <https://doi.org/10.1002/glia.22727>
- Yang, J., Zhang, L., Yu, C., Yang, X.-F., & Wang, H. (2014). Monocyte and macrophage differentiation: Circulation inflammatory monocyte as biomarker for inflammatory diseases. *Biomarker Research*, *2*(1), 1. <https://doi.org/10.1186/2050-7771-2-1>
- Yu, G., Wang, L.-G., Han, Y., & He, Q.-Y. (2012). clusterProfiler: An R package for comparing biological themes among gene clusters. *OMICS: A Journal of Integrative Biology*, *16*(5), 284–287. <https://doi.org/10.1089/omi.2011.0118>
- Zeng, H. Y., Green, W. R., & Tso, M. O. (2008). Microglial activation in human diabetic retinopathy. *Archives of Ophthalmology*, *126*, 227–232. <https://doi.org/10.1001/archophthalmol.2007.65>

#### SUPPORTING INFORMATION

Additional supporting information may be found online in the Supporting Information section at the end of this article.

**How to cite this article:** Boeck M, Thien A, Wolf J, et al. Temporospatial distribution and transcriptional profile of retinal microglia in the oxygen-induced retinopathy mouse model. *Glia*. 2020;68:1859–1873. <https://doi.org/10.1002/glia.23810>